RESEARCH ARTICLE | NOVEMBER 01 2024

Comparing parameterized and self-consistent approaches to *ab initio* cavity quantum electrodynamics for electronic strong coupling

Special Collection: Polaritonics for Next Generation Materials

Ruby Manderna ; Nam Vu ; Jonathan J. Foley, IV

J. Chem. Phys. 161, 174105 (2024)
https://doi.org/10.1063/5.0230565

The Journal of Chemical Physics ARTICLE pubs.aip.org/aip/jcp

Comparing parameterized and self-consistent approaches to *ab initio* cavity quantum electrodynamics for electronic strong coupling

Cite as: J. Chem. Phys. 161, 174105 (2024); doi: 10.1063/5.0230565
Submitted: 24 July 2024 • Accepted: 14 October 2024 •
Published Online: 1 November 2024

Ruby Manderna, Nam Vu, and Jonathan J. Foley IV[a)]

AFFILIATIONS

Department of Chemistry, University of North Carolina Charlotte, 9201 University City Bldv, Charlotte, North Carolina 07470A, USA

Note: This paper is part of the JCP Special Topic on Polaritonics for Next Generation Materials.
[a)]**Author to whom correspondence should be addressed:** jfoley19@charlotte.edu

ABSTRACT

Molecules under strong or ultra-strong light–matter coupling present an intriguing route to modify chemical structure, properties, and reactivity. A rigorous theoretical treatment of such systems requires handling matter and photon degrees of freedom on an equal quantum mechanical footing. In the regime of molecular electronic strong or ultra-strong coupling to one or a few molecules, it is desirable to treat the molecular electronic degrees of freedom using the tools of *ab initio* quantum chemistry, yielding an approach referred to as *ab initio* cavity quantum electrodynamics (ai-QED), where the photon degrees of freedom are treated at the level of cavity QED. We analyze two complementary approaches to ai-QED: (1) a parameterized ai-QED, a two-step approach where the matter degrees of freedom are computed using existing electronic structure theories, enabling the construction of rigorous ai-QED Hamiltonians in a basis of many-electron eigenstates, and (2) self-consistent ai-QED, a one-step approach where electronic structure methods are generalized to include coupling between electronic and photon degrees of freedom. Although these approaches are equivalent in their exact limits, we identify a disparity between the projection of the two-body dipole self-energy operator that appears in the parameterized approach and its exact counterpart in the self-consistent approach. We provide a theoretical argument that this disparity resolves only under the limit of a complete orbital basis and a complete many-electron basis for the projection. We present numerical results highlighting this disparity and its resolution in a particularly simple molecular system of helium hydride cation, where it is possible to approach these two complete basis limits simultaneously. In this same helium hydride system, we examine and compare the practical issue of the computational cost required to converge each approach toward the complete orbital and many-electron bases limit. Finally, we assess the aspect of photonic convergence for polar and charged species, finding comparable behavior between parameterized and self-consistent approaches.

I. INTRODUCTION

Strong interactions between molecular electronic and photonic degrees of freedom (i.e., electronic strong and ultra-strong coupling) can fundamentally alter chemical structure, reactivity, and phenomenology.[1–23] Predictive theoretical and computational models for molecules under electronic strong coupling must capture the quantum nature of electronic and photonic degrees of freedom. In the limit of molecular electronic strong or ultra-strong coupling to one or a few molecules, it is desirable to treat the molecular electronic degrees of freedom using the tools of *ab initio* quantum chemistry, yielding an approach referred to as *ab initio* cavity quantum electrodynamics (ai-QED), where the photon degrees of freedom are treated at the level of cavity quantum electrodynamics. Two complementary approaches have emerged for ai-QED: (1) parameterized CQED[20,23–27] (pQED), a two-step approach where the matter degrees of freedom are computed using existing electronic structure theories, enabling one to build rigorous ai-QED Hamiltonians in a basis of many-electron eigenstates, and (2) self-consistent CQED[19,28–51] (scQED), a one-step approach where electronic structure methods are generalized to include coupling between electrons and photon degrees of freedom.

Although these approaches are equivalent in their exact limits, it is practically impossible to reach these exact limits for the vast majority of physically relevant systems. Outside their exact limits, the variety of approximations inherent in electronic structure calculations makes it quite difficult to assess these two approaches on equal footing. In this work, we attempt to provide a fair assessment of these two approaches based upon simple analysis of their underlying formalisms and through comparable numerical results approaching exact limits. To this end, we implement two approaches to pQED and scQED using full configuration interaction (FCI) to parameterize the former and a self-consistent QED-FCI scheme for the latter. Analysis of the formalism of both approaches shows that these approaches are indeed equivalent in the limit of a complete orbital and many-electron basis, but have a key disparity in a quadratic light–matter coupling term, known as the dipole self-energy, outside this limit. While scQED utilizes the exact form of the dipole self-energy operator in a given orbital basis, the projected dipole self-energy that arises in pQED is inexact, except for in a complete orbital and many-electron basis. We present numerical results highlighting this disparity and its resolution in a particularly simple molecular system of helium hydride cation, where it is possible to approach these two complete basis limits simultaneously. In this same helium hydride system, we examine and compare the practical issue of computational cost required to converge each approach toward the complete orbital and many-electron bases limit. Finally, we assess the aspect of photonic convergence for polar and charged species, finding comparable behavior between parameterized and self-consistent approaches.

II. THEORY

We will discuss two complementary approaches to ai-QED that seek to find accurate eigenstates of the Pauli-Fierz (PF) Hamiltonian[52,53] represented in the length gauge and within the dipole and Born–Oppenheimer approximations. Here, we write down the Pauli-Fierz Hamiltonian for a molecular system coupled to a single photonic mode in atomic units as

$$\hat{H}_{\mathrm{PF}} = \hat{H}_e + \omega \hat{b}^\dagger \hat{b} - \sqrt{\frac{\omega}{2}}\hat{d}(\hat{b}^\dagger + \hat{b}) + \frac{1}{2}\hat{d}^2. \tag{1}$$

In Eq. (1), $\hat{H}_e$ is the standard electronic Hamiltonian within the Born–Oppenheimer approximation;[54] $\omega \hat{b}^\dagger \hat{b}$ is the bare Hamiltonian for the photon mode, where ω represents the frequency; and $\hat{b}^\dagger$ and $\hat{b}$ are raising and lowering operators for the photon mode, respectively. The final two terms capture interactions between the photonic and electronic degrees of freedom. In these interaction terms, known as the bilinear coupling and the quadratic dipole self-energy, $\hat{d} = \boldsymbol{\lambda} \cdot \hat{\boldsymbol{\mu}}$ couples the field associated with the photon mode to the molecular dipole operator.[55]

The formulation of several ai-QED methods (e.q. QED-Hartree–Fock, QED-CC, and QED-CASCI) has been performed after transforming Eq. (1) to the coherent-state basis,[36,42,44,56]

$$\hat{H}_{\mathrm{CS}} = \hat{H}_e + \omega \hat{b}^\dagger \hat{b} - \sqrt{\frac{\omega}{2}}[\hat{d}_e - \langle \hat{d}_e \rangle](\hat{b}^\dagger + \hat{b}) + \frac{1}{2}[\hat{d}_e - \langle \hat{d}_e \rangle]^2. \tag{2}$$

This follows from a unitary transformation of the Pauli-Fierz Hamiltonian,

$$\hat{H}_{\mathrm{CS}} = \hat{U}_{\mathrm{CS}} \hat{H}_{\mathrm{PF}} \hat{U}_{\mathrm{CS}}^\dagger, \tag{3}$$

where the unitary coherent state transformation is defined as

$$\hat{U}_{\mathrm{CS}} = \exp\left(z(\hat{b}^\dagger - \hat{b})\right). \tag{4}$$

The parameter z may be computed as

$$z = \frac{-\langle \hat{d} \rangle}{\sqrt{2\omega}}. \tag{5}$$

Often, $\langle \hat{d} \rangle$ is computed for a given electronic reference state, for example, in the QED-HF reference in scQED formulations.[35,36] Here, we will also investigate the CS transformation of the projected Pauli-Fierz Hamiltonian for a pQED formulation, where $\langle \hat{d} \rangle$ will be computed in the adiabatic many-electron basis. We note that within the Born–Oppenheimer approximation, the nuclear contribution in $\langle \hat{d} \rangle$ exactly cancels with the nuclear contribution to $\hat{d}$, hence we write Eq. (2) with $\hat{d}_e$ and $\langle \hat{d}_e \rangle$ to denote only the electronic contribution to both terms.

We can approach the solution to Eqs. (1) or (2) in two complementary ways. The pQED approach will first find the adiabatic eigenstates that define $\hat{H}_e|\psi_\alpha(\mathbf{R})\rangle = E_\alpha(\mathbf{R})|\psi_\alpha(\mathbf{R})\rangle$ using standard quantum chemistry tools, where $\mathbf{R}$ denotes the coordinates of the nuclei, which are fixed within the Born–Oppenheimer approximation. In a subsequent step, one builds a Hamiltonian matrix from Eqs. (1) or (2) in the basis of direct products between these adiabatic eigenstates and photonic Fock states. The approach denoted scQED will seek the eigenstates of Eqs. (1) or (2) directly in a product basis of many-electron states (Slater determinants in this work) and photonic Fock states.

Both approaches can reach an exact limit. For pQED, the exact limit can be achieved when one builds Eqs. (1) or (2) in the complete basis of *exact* adiabatic eigenstates and photonic Fock states. Of course, it is practically impossible to reach this limit for most molecular systems, so a practical approach will consider building the pQED Hamiltonian in a truncated basis of many-electron states. In practice, this basis of adiabatic eigenstates is not only incomplete, but the states themselves are inexact because they results from an approximate quantum chemistry method. The approximations inherent in practical quantum chemistry calculations include truncation of the single-particle basis (e.g., using a finite number of Gaussian-type orbital basis functions), and truncation of the many-electron space through, for example, truncation of the excitation rank in a configuration interaction (CI) ansatz. The exact limit of the scQED approach includes a complete single-particle basis for the electronic subsystem, a complete many-electron basis (through, e.g., an FCI ansatz that includes all excited electronic configurations, often represented as Slater determinants or configuration state functions), and a complete photonic Fock space, which is also not practical in general. Our goal in this current paper is to study the convergence properties of both methods toward their exact limits and to point out quantitative differences that arise outside of the complete basis limit.

A. pQED

In the pQED approach, we can build Eqs. (1) or (2) in a product basis of adiabatic electronic states $|\psi_\alpha\rangle$ and photonic Fock states $|n\rangle$ corresponding to n photons in the cavity mode, such that the coupled eigenstates can be expressed as linear combinations of these product basis states,

$$|\Psi_{\text{ep}}\rangle = \sum_n \sum_\alpha C_{\alpha,n}|\psi_\alpha\rangle \otimes |n\rangle. \tag{6}$$

Here, the dependence of the adiabatic many-electron states on the nuclear coordinate $\mathbf{R}$ is implied. We briefly review the expressions that arise in the pQED approach leading to a matrix representation of Eq. (1) in a truncated basis of adiabatic electronic states; the salient differences that arise in the matrix form of Eq. (2) are pointed out at the end of this development.

We define the following projection operator:

$$\hat{\mathcal{P}} = \sum_\alpha^{N_{\text{el}}} |\psi_\alpha\rangle\langle\psi_\alpha|, \tag{7}$$

which defines the truncation of the full electronic Hilbert space to a subspace of N_{el} states. We can also define the complementary projector $\hat{\mathcal{Q}}$, such that these two operators obey

$$\hat{\mathbf{1}} = \hat{\mathcal{P}} + \hat{\mathcal{Q}}, \tag{8}$$

where the resolution of the identity is satisfied by the complete electronic Hilbert space. Following the discussion by Huo and co-workers, we can think of the truncated version of Eq. (1) as arising from transformation with a projected Power–Zienau–Woolley (PZW) operator from the minimal coupling Hamiltonian.[57] The projected PZW operator has the form

$$\mathcal{U}_{\text{PZW}} = e^{-\frac{i}{\hbar}\hat{\mathcal{P}}\hat{\boldsymbol{\mu}}\hat{\mathcal{P}}\cdot\hat{\mathbf{A}}}, \tag{9}$$

where $\hat{\mathcal{P}}\hat{\boldsymbol{\mu}}\hat{\mathcal{P}}$ denotes the matter dipole operator projected onto the electronic subspace and $\hat{\mathbf{A}}$ is the vector potential operator, which only acts on the photonic subspace and is not projected. From this perspective, we can write the projected Hamiltonian as follows:

$$\mathcal{H}_{\text{PF}} = \mathcal{H}_{\text{e}} + \mathcal{H}_{\text{cav}} + \mathcal{H}_{\text{blc}} + \mathcal{H}_{\text{dse}}, \tag{10}$$

where the calligraphic operators denote they have been projected into a subspace defined by $\hat{\mathcal{P}}$, that is, $\mathcal{H} = \hat{\mathcal{P}}\hat{H}\hat{\mathcal{P}}$. It is important to note that the projector only acts on matter operators, so we need only consider the impact of truncation on $\hat{H}_{\text{e}}$, $\hat{H}_{\text{blc}}$, and $\hat{H}_{\text{dse}}$. The projected molecular electronic Hamiltonian has the form

$$\hat{\mathcal{P}}\hat{H}_{\text{e}}\hat{\mathcal{P}} = \sum_\alpha^{N_{\text{el}}} E_\alpha|\psi_\alpha\rangle\langle\psi_\alpha|, \tag{11}$$

where $E_\alpha = E_\alpha(\mathbf{R})$ are the energy eigenvalues of the adiabatic eigenstates noted in Eq. (6). The bilinear coupling terms has the form

$$\hat{\mathcal{P}}\hat{H}_{\text{blc}}\hat{\mathcal{P}} = -\sqrt{\frac{\omega}{2}}\hat{\mathcal{P}}\hat{d}\hat{\mathcal{P}}\left(\hat{b}^\dagger + \hat{b}\right) = -\sqrt{\frac{\omega}{2}}\sum_{\alpha\beta}^{N_{\text{el}}} d_{\alpha\beta}|\psi_\alpha\rangle\langle\psi_\beta|\left(\hat{b}^\dagger + \hat{b}\right), \tag{12}$$

where $d_{\alpha\beta} = \langle\psi_\alpha|\hat{d}|\psi_\beta\rangle$ results from dotting the coupling vector into the transition dipole moment between adiabatic states α and β or the total dipole moment of state α when $\alpha = \beta$; this quantity also depends explicitly on the nuclear coordinates, but we are suppressing the dependence on $\mathbf{R}$ in our notation for simplicity. The transition dipole moments are purely electronic, while the total dipole moments have both an electronic and nuclear contribution. Finally, the dipole self-energy has the form

$$\hat{\mathcal{P}}\hat{H}_{\text{dse}}\hat{\mathcal{P}} = \frac{1}{2}\hat{\mathcal{P}}\hat{d}\hat{\mathcal{P}}\hat{\mathcal{P}}\hat{d}\hat{\mathcal{P}} = \frac{1}{2}\sum_{\alpha\beta\gamma}^{N_{\text{el}}} d_{\alpha\gamma}d_{\gamma\beta}|\psi_\alpha\rangle\langle\psi_\beta|. \tag{13}$$

If we build a matrix from the projected Pauli-Fierz matrix (here, denoted $\mathbf{H}_{\text{PF}}$) in the basis given in Eq. (6), we have the general structure,

$$\mathbf{H}_{\text{PF}} = \begin{bmatrix} \mathbf{E}+\mathbf{D} & \mathbf{d} & 0 & \dots & 0 & 0 \\ \mathbf{d} & \mathbf{E}+\mathbf{D}+\boldsymbol{\Omega} & \sqrt{2}\mathbf{d} & \dots & 0 & 0 \\ 0 & \sqrt{2}\mathbf{d} & \mathbf{E}+\mathbf{D}+2\boldsymbol{\Omega} & \dots & 0 & 0 \\ \vdots & \vdots & \vdots & \ddots & \vdots & \vdots \\ 0 & 0 & 0 & \dots & \mathbf{E}+\mathbf{D}+(N_{\text{p}}-2)\boldsymbol{\Omega} & \sqrt{(N_{\text{p}}-1)}\mathbf{d} \\ 0 & 0 & 0 & \dots & \sqrt{(N_{\text{p}}-1)}\mathbf{d} & \mathbf{E}+\mathbf{D}+(N_{\text{p}}-1)\boldsymbol{\Omega} \end{bmatrix}. \tag{14}$$

Here, the elements of $\mathbf{E}$ are given by

$$E_{\alpha n,\beta m} = \langle n|\langle\psi_\alpha|\mathcal{H}_{\text{e}}|\psi_\beta\rangle|m\rangle = E_\alpha\delta_{\alpha\beta}\delta_{nm}; \tag{15}$$

the elements of $\mathbf{D}$ are

$$D_{\alpha n,\beta m} = \langle n|\langle\psi_\alpha|\mathcal{H}_{\text{dse}}|\psi_\beta\rangle|m\rangle = \frac{1}{2}\sum_\gamma^{N_{\text{el}}} d_{\alpha\gamma}d_{\gamma\beta}\delta_{nm}; \tag{16}$$

the elements of $\mathbf{d}$ are

$$d_{\alpha n,\beta m} = \langle n|\langle\psi_\alpha|\mathcal{H}_{\text{blc}}|\psi_\beta\rangle|m\rangle = -\sqrt{\frac{\omega}{2}}d_{\alpha\beta}\eta_{nm}, \tag{17}$$

where $\eta_{nm} = \sqrt{m+1}\delta_{n,m+1} + \sqrt{m}\delta_{n,m-1}$. The elements of $\boldsymbol{\Omega}$ are

$$\Omega_{\alpha n,\beta m} = \langle n|\langle\psi_\alpha|\mathcal{H}_{\text{cav}}|\psi_\beta\rangle|m\rangle = m\omega\delta_{\alpha\beta}. \tag{18}$$

The structure of the matrix in Eq. (14) reflects the Kronecker delta functions that appear in the respective block equations. The structure of the matrix of the projected version of Eq. (2) is comparable to that in Eq. (14), with the only substantive difference being that the matrix elements of $\hat{\mathcal{P}}\hat{d}\hat{\mathcal{P}}$ are offset by $\langle\hat{d}\rangle$, i.e., $d_{\alpha\beta} - \langle\hat{d}\rangle\delta_{\alpha\beta}$. We have a choice in what state to compute $\langle\hat{d}\rangle$, and in this work, we choose the ground state of the uncoupled system unless otherwise specified.

B. scQED

In the self-consistent approach, one adapts their quantum chemistry method to directly include the terms beyond $\hat{H}_e$ in Eqs. (1) or (2). In this approach, we begin with the exact matter operators, which will be denoted in an ordinary font, not a calligraphic font like the projected matter operators in Subsection II A.

An scQED approach can be formulated based on the following configuration interaction ansatz for the mixed electronic-photonic eigenstates:

$$|\Psi_{ep}\rangle = \sum_n \sum_I C_{I,n}|\Phi_I\rangle \otimes |n\rangle, \tag{19}$$

where $|\Phi_I\rangle$ represents an electronic Slater determinant, $|n\rangle$ is a photon-number state, and $C_{I,n}$ is an expansion coefficient.[44] Then, an scQED approach can be formulated as a matrix diagonalization problem, where Eqs. (1) or (2) is built in the basis of product states in Eq. (19). The matrix representation of Eq. (1) (here denoted $\mathbf{H}_{\text{PF-CI}}$) has a similar structure as Eq. (14),

$$\mathbf{H}_{\text{PF-CI}} = \begin{bmatrix} \mathbf{A}+\mathbf{\Delta} & \mathbf{G} & 0 & \dots & 0 & 0 \\ \mathbf{G} & \mathbf{A}+\mathbf{\Delta}+\mathbf{\Omega} & \sqrt{2}\mathbf{G} & \dots & 0 & 0 \\ 0 & \sqrt{2}\mathbf{G} & \mathbf{A}+\mathbf{\Delta}+2\mathbf{\Omega} & \dots & 0 & 0 \\ \vdots & \vdots & \vdots & \ddots & \vdots & \vdots \\ 0 & 0 & 0 & \dots & \mathbf{A}+\mathbf{\Delta}+(N_p-2)\mathbf{\Omega} & \sqrt{(N_p-1)}\mathbf{G} \\ 0 & 0 & 0 & \dots & \sqrt{(N_p-1)}\mathbf{G} & \mathbf{A}+\mathbf{\Delta}+(N_p-1)\mathbf{\Omega} \end{bmatrix}. \tag{20}$$

The elements of $\mathbf{A}$ are

$$A_{In,Jm} = \langle n|\langle\Phi_I^e|\hat{H}_e|\Phi_J^e\rangle|m\rangle = \langle\Phi_I^e|\hat{H}_e|\Phi_J^e\rangle\delta_{nm}. \tag{21}$$

The elements of $\mathbf{\Delta}$ are

$$\begin{aligned}\Delta_{In,Jm} &= \frac{1}{2}\langle n|\langle\Phi_I^e|\hat{d}^2|\Phi_J^e\rangle|m\rangle \\ &= \frac{1}{2}\Big(\langle\Phi_I^e|\hat{d}_e{}^2|\Phi_J^e\rangle + 2d_n\langle\Phi_I^e|\hat{d}_e|\Phi_J^e\rangle + d_n^2\delta_{IJ}\Big)\delta_{nm},\end{aligned} \tag{22}$$

where $\hat{d}_e$ denotes the electronic contribution to $\hat{d}$ and d_n denotes the nuclear contribution. The matrix elements of $\mathbf{G}$ are

$$\begin{aligned}G_{In,Jm} &= -\sqrt{\frac{\omega}{2}}\langle n|\langle\Phi_I^e|\ \hat{d}\ (\hat{b}^\dagger + \hat{b})|\Phi_J^e\rangle|m\rangle \\ &= -\sqrt{\frac{\omega}{2}}\langle\Phi_I^e|\hat{d}|\Phi_J^e\rangle\eta_{nm}.\end{aligned} \tag{23}$$

Finally, the elements of $\mathbf{\Omega}$ are given by

$$\Omega_{In,Jm} = \langle n|\langle\Phi_I^e|\omega\hat{b}^\dagger\hat{b}|\Phi_J^e\rangle|m\rangle = m\omega\delta_{IJ}\delta_{nm}. \tag{24}$$

More explicit expressions for these matrix elements, as well as those for the elements corresponding to Eq. (2), can be found in Ref. 44.

C. Dipole self-energy in pQED vs scQED

A key difference between practical implementations of pQED and scQED resides in the treatment of the dipole self-energy, specifically arising from the product of electronic operators in $\hat{d}_e{}^2$.

In the scQED approach, we are not starting with any specific state truncation in mind, and so our scQED Hamiltonian is written in terms of exact electronic operators. In the first quantization, we can expand $\hat{d}_e{}^2$ as

$$\hat{d}_e{}^2 = \sum_{i\neq j} d_e(i)\ d_e(j) + \sum_i [d_e(i)]^2, \tag{25}$$

where i and j represent different electronic coordinates; hence we see that the dipole self-energy operator contains both a one-electron contribution and a two-electron contribution. The one-electron contribution can be recognized as the negative of the quadrupole operator multiplied by coupling vector components. A practical scQED approach will depend on introducing an orbital basis (e.g., an orthonormal spin orbital basis). In this case, we can write the right-hand side of Eq. (25) in second-quantized notation as

$$\hat{d}_e{}^2 = \sum_{pqrs} d_{pq}d_{rs}\hat{a}_p^\dagger\hat{a}_r^\dagger\hat{a}_s\hat{a}_q - \sum_{pq} Q_{pq}\hat{a}_p^\dagger\hat{a}_q, \tag{26}$$

where $\hat{a}^\dagger$ and $\hat{a}$ represent fermionic creation and annihilation operators, respectively. The symbols d_{pq} and Q_{pq} represent modified electric dipole and electric quadrupole integrals, respectively.[44] We can see that this form of the dipole self-energy operator employed in the scQED approach maintains the exact structure to within the discretization error introduced by a finite orbital basis.

Let us turn to the projected dipole self-energy operator that arises in pQED, which as we saw in Eq. (13), containing a product of projected modified dipole operators,

$$\begin{aligned}\hat{\mathcal{P}}\hat{d}_e\hat{\mathcal{P}}\hat{\mathcal{P}}\hat{d}_e\hat{\mathcal{P}} &= \sum_{\alpha\gamma\delta\beta}^{N_{el}} |\psi_\alpha\rangle\langle\psi_\alpha|\hat{d}_e|\psi_\gamma\rangle\langle\psi_\gamma|\psi_\delta\rangle\langle\psi_\delta|\hat{d}_e|\psi_\beta\rangle\langle\psi_\beta| \\ &= \sum_{\alpha\gamma\beta}^{N_{el}} |\psi_\alpha\rangle\langle\psi_\alpha|\hat{d}_e|\psi_\gamma\rangle\langle\psi_\gamma|\hat{d}_e|\psi_\beta\rangle\langle\psi_\beta| \\ &= \sum_{\alpha\gamma\beta}^{N_{el}} d_{\alpha\gamma}d_{\gamma\beta}|\psi_\alpha\rangle\langle\psi_\beta|, \end{aligned} \tag{27}$$

$$\hat{\mathcal{P}}\hat{d}_e\hat{\mathcal{P}}\hat{\mathcal{P}}\hat{d}_e\hat{\mathcal{P}} = \sum_{\alpha\gamma\beta}^{N_{el}} d_{\alpha\gamma}d_{\gamma\beta}|\psi_\alpha\rangle\langle\psi_\beta|. \tag{28}$$

We note that we can express Eq. (28) in the same orbital basis as in Eq. (26) by noting that the adiabatic electronic states can be written as a linear expansion of Slater determinants as

$$|\psi_\alpha\rangle = \sum_I c_I|\Phi_I\rangle, \tag{29}$$

where each $|\Phi_I\rangle$ can be written as an antisymmetrized product of canonical molecular orbitals. These Slater determinants include the Hartree–Fock reference and all possible number conserving excitations from it. We can then denote the matrix elements $d_{\alpha\beta}$ in this adiabatic basis as

$$\langle\psi_\alpha|\hat{d}_e|\psi_\beta\rangle = \sum_{IJ} c_I^* c_J\langle\Phi_I|\hat{d}_e|\Phi_J\rangle = \sum_{IJ}\sum_{pq} c_I^* c_J\langle\Phi_I|\hat{a}_p^\dagger\hat{a}_q|\Phi_J\rangle d_{pq}, \tag{30}$$

where the matrix elements $\langle\Phi_I|\hat{a}_p^\dagger\hat{a}_q|\Phi_J\rangle$ can be evaluated using the Slater–Condon rules.[54,58] In general, these matrix elements will be non-zero only if determinants $|\Phi_I\rangle$ and $|\Phi_J\rangle$ differ in the occupation of zero or one orbitals. With this expression for the matrix elements of $\hat{d}_e$ in the adiabatic basis in terms of molecular orbitals in mind, we can express the product of matrix elements appearing in Eq. (28) as

$$d_{\alpha\gamma}d_{\gamma\beta} = \sum_{IJK}\sum_{pqrs} c_I^* c_J c_J^* c_K\langle\Phi_I|\hat{a}_p^\dagger\hat{a}_q|\Phi_J\rangle\langle\Phi_J|\hat{a}_r^\dagger\hat{a}_s|\Phi_K\rangle d_{pq}d_{rs}. \tag{31}$$

Notably, the projected dipole self-energy is missing the quadrupole terms that are present in the exact dipole self-energy operator. Therefore, in addition to the discretization error that arises from a finite orbital basis, the exact structure of the dipole self-energy is lost upon projection onto an incomplete electronic subspace. We will see that this generally leads to a different variational problem, whereby the pQED energies can converge to different solutions than the scQED approach.

We now show that this difference resolves itself in the limit of a complete orbital and many-electron basis. First, we will show that the quadrupole term in the exact dipole self-energy operator vanishes in the limit of a complete orbital basis. As a first step, we utilize the anticommutation relations in the two-electron part of Eq. (26),

$$\begin{aligned}\sum_{pqrs} d_{pq}d_{rs}\hat{a}_p^\dagger\hat{a}_r^\dagger\hat{a}_s\hat{a}_q &= -\sum_{pqrs} d_{pq}d_{rs}\hat{a}_p^\dagger[\delta_{qr} - \hat{a}_q\hat{a}_r^\dagger]\hat{a}_s \\ &= \sum_{pq} d_{pq}\hat{a}_p^\dagger\hat{a}_q\sum_{rs} d_{rs}\hat{a}_r^\dagger\hat{a}_s - \sum_{pqr} d_{pr}d_{rq}\hat{a}_p^\dagger\hat{a}_q. \end{aligned} \tag{32}$$

We can now substitute the last line of Eq. (32) into Eq. (26),

$$\hat{d}_e{}^2 = \sum_{pq} d_{pq}\hat{a}_p^\dagger\hat{a}_q\sum_{rs} d_{rs}\hat{a}_r^\dagger\hat{a}_s - \sum_{pq}\left(\sum_r d_{pr}d_{rq} + Q_{pq}\right)\hat{a}_p^\dagger\hat{a}_q. \tag{33}$$

As a second step, we can insert a resolution of the identity into $\sum_r d_{pr}d_{rq}$ when the orbital basis is complete, which gives

$$\sum_r^\infty d_{pr}d_{rq} = -Q_{pq}, \tag{34}$$

which means that when the orbital basis is complete, the quadrupole contribution to the dipole self-energy vanishes, and we have

$$\hat{d}_e^2 = \sum_{pq} d_{pq}\hat{a}_p^\dagger\hat{a}_q\sum_{rs} d_{rs}\hat{a}_r^\dagger\hat{a}_s. \tag{35}$$

Finally, we note that in the pQED approach, when the dipole self-energy is projected onto an incomplete electronic subspace, the product of $\hat{d}$ operators is replaced by the product of matrix elements of those operators. However, in the limit that the electronic subspace is complete, we have $\hat{\mathcal{P}} = \hat{1}$ and we resolve the projected dipole self-energy into a product of $\hat{d}$ operators,

$$\hat{\mathcal{P}}\hat{d}_e\hat{\mathcal{P}}\hat{\mathcal{P}}\hat{d}_e\hat{\mathcal{P}} = \hat{d}_e\hat{d}_e. \tag{36}$$

Therefore, we conclude that the exact and projected dipole self-energy operators agree in the limit that both the complete orbital and many-electron basis limits have been reached.

III. COMPUTATIONAL DETAILS

The selection of model systems for comparing the convergence behavior of pQED and scQED approaches includes a two-electron system (helium hydride cation, HeH^+), a four electron system (lithium hydride, LiH) that is neutral but polar, and a ten electron system (hydroxide anion, OH^-); for all cases, we consider closed-shell singlet states. We represent the HeH^+ system in the cc-pVXZ[59] basis sets with $X \in D, T, Q$ to systematically approach the complete orbital basis limit; we represent LiH in a 6-311G basis set[60] and OH^- in a 6-31G basis set. We perform all calculations, including computing the adiabatic many electron states and dipole matrix elements for pQED calculations, and the scQED calculations, utilizing the qed-ci package developed by the authors,[61] which obtains electron integrals through the Psi4Numpy interface with the Psi4 quantum chemistry package.[62,63]

A glossary of abbreviations and terms used to discuss the results is presented in Table I.

TABLE I. Glossary of acronyms used to describe different methodologies used in this work.

pQED	General approach where Eqs. (1) or (2) are built in a product basis of adiabatic electronic states and photonic Fock states
scQED	General approach where Eqs. (1) or (2) are built in a product basis of slater determinants and photonic Fock states
pPF(N_{el}, N_p)	Projection of Eq. (1) onto a basis of N_{el} adiabatic many electron states, including the electronic ground state, and N_p photonic Fock states
PF-FCI-N_p	Self-consistent variational solution to Eq. (1) in a product basis of all excited slater determinants and N_p photonic Fock states
pCS(N_{el}, N_p)	Projection of Eq. (2) onto a basis of N_{el} adiabatic many electron states, including the electronic ground state, and N_p photonic Fock states
CS-FCI-N_p	Self-consistent variational solution to Eq. (2) in a product basis of all excited Slater determinants and N_p photonic Fock states
pRabi(N_{el}, N_p)	Projection of Eq. (1) without the dipole self-energy term onto a basis of N_{el} adiabatic many electron states, including the electronic ground state, and N_p photonic Fock states
Rabi-FCI-N_p	Self-consistent variational solution to Eq. (1) without the dipole self-energy in a product basis of all excited Slater determinants and N_p photonic Fock states

IV. RESULTS

A. Helium hydride ion (HeH^+)

HeH^+ is a two-electron system shown in Fig. 1 that has a permanent ground-state dipole moment and a dipole-allowed optical transition ($S_0 \rightarrow S_2$ with transition energy of 26.1 eV), which will permit us to study the behavior of the dipole self-energy on the ground and polariton states using scQED and pQED approaches as we approach the complete basis limit. We optimize the geometry of this system at the FCI/cc-pVTZ level; at this level, the equilibrium bond length is ~0.776 Å and the dipole moment has a magnitude of 1.73 D along the internuclear axis. We fix the nuclei of this system so that its center of mass resides at the origin of the cavity coordinate system for all calculations. We study the ground state and polariton states at the PF-FCI and pPF levels using cc-pVXZ basis sets, where X is D, T, and Q, to progress toward the complete orbital basis limit (Table II).

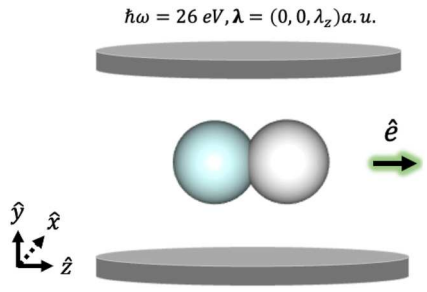

FIG. 1. Schematic of HeH^+ coupled to a cavity mode polarized along the internuclear axis (z) and tuned to the first optically allowed transition from $S_0 \rightarrow S_2$ at ~26 eV.

TABLE II. Comparison of Rabi splitting as predicted by PF-FCI-10/cc-pVXZ and pPF(N_{el}, 10)/cc-pVXZ methods for HHe^+ when $\hbar\omega$ = 26 eV and λ_z = 0.1 a.u. The error reported in meV is defined as the Rabi splitting predicted by the pPF approach minus the Rabi splitting predicted by the PF-FCI approach.

	Rabi splitting (eV)		
Basis set	PF-FCI	pPF	Error (meV)
cc-pVDZ	2.922	2.905	−17.26
cc-pVTZ	3.033	3.026	−7.64
cc-pVQZ	3.041	3.037	−4.76

We first report the absolute energy error of the ground state energy as computed by pPF(N_{el}, 10) relative to PF-FCI-10 for each basis set, where N_{el} is the number of many-electron basis states used to parameterize the pPF Hamiltonian (see Fig. 2). We find that N_p = 10 is more than sufficient to converge the photonic Fock space and so PF-FCI-10 provides the exact energies for this system in a given orbital basis. We see that the energy error decreases as we increase N_{el} in a given orbital basis and also decreases with increasing size of the orbital basis. The energy error of pPF(N_{el}, 10)/cc-pVDZ converges to ~10 microhartrees in the limit that all the FCI states are used to parameterize the Hamiltonian, while the energy error of pPF(N_{el}, 10)/cc-pVQZ converges to

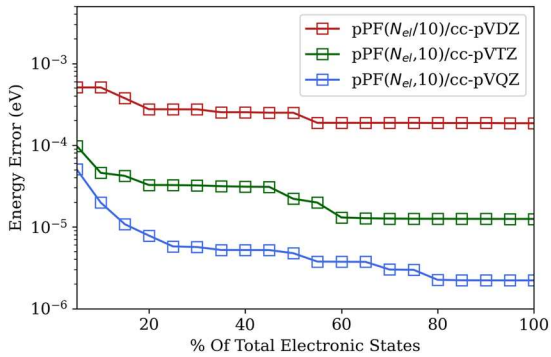

FIG. 2. Absolute error of the pPF(N_{el}, 10) ground state energy relative to the PF-FCI-10 ground state energy computed within the cc-pVDZ, cc-pVTZ, and cc-pVQZ basis sets, where we plot this error as a function of the percentage of the FCI electronic states used to parameterize the pPF(N_{el}, 10) method. The photon frequency in each case is tuned to the $S_0 \rightarrow S_2$ transition, and λ_z is fixed at 0.02 a.u.

0.1 microhartrees in the comparable limit (see Fig. 2). These results are consistent with the argument that the projected dipole self-energy approaches the exact dipole self-energy in the limit that both the orbital and many-electron basis are complete. We also note that the fraction of electronic states needed for energy convergence increases from around 50% in cc-pVDZ to 80% in cc-pVQZ.

Similarly, in Fig. 3, the curves represent the absolute energy error vs coupling strength of the pPF(N_{el}, 10) ground state energies in each basis set, where we have fixed N_{el} at the value where we observed the energy converge in Fig. 2. All the methods show errors of less than a microhartree for coupling strengths smaller than ~0.01 a.u. but show increasing errors as the coupling strength increases. For pPF(2880, 10)/cc-pVQZ, we see a microhartree error with the largest coupling strength (λ_z = 0.1), and we see ~100 microhartree error for pPF(60, 10)/cc-pVDZ at this coupling strength. Because the dipole self-energy is quadratic in the coupling strength, we expect to see that the disparity between pQED and scQED will become more dramatic as the coupling strength increases. The progression shown in Fig. 3 shows that differences between the exact and projected dipole self-energy operators have not been fully resolved even when using a cc-pVQZ orbital basis and 2880 many-electron states. In particular, this arises because the statement $\sum_r^\infty d_{pr}d_{rq} = -Q_{pq}$ does not hold, meaning the one electron residual of Eq. (30) does not vanish. We compute the magnitude of this residual by tracing both the Q matrix and the product of d matrices against the converged one electron reduced density matrix for the ground state of the PF-FCI-10 Hamiltonians in Fig. 4. Indeed, we see that this residual increases quadratically with $\boldsymbol{\lambda}$, but also converges toward zero as we approach the complete basis limit. There is still a non-zero residual for the cc-pVQZ results, so the complete basis limit has not been reached in this case.

In Figs. 5–7, we show both ground state and polariton excitation energies of the HeH^+ system computed in all three basis sets with the pPF and PF-FCI approaches for varying values of coupling strength. The ground state energies are plotted relative to the uncoupled ground state $E_g(\lambda) - E_g(\lambda = 0)$, where the uncoupled ground state energy is equivalent to the full configuration interaction ground state energy in a given basis set. The excitation energies are defined as the energy of a polariton state at a given coupling strength minus the ground state energy at the same coupling strength, $E_{pol}(\lambda) - E_g(\lambda)$. An interesting feature of this study is that the pPF (ground state and polariton) energies are consistently a lower bound on the PF-FCI energies, and each approaches the corresponding PF-FCI energy from below as we approach the complete basis limit. We emphasize that because the projected dipole self-energy is inexact outside of the complete basis limit, the pPF and PF-FCI approaches provide a variational approach for two distinct Hamiltonians, and so we cannot make any concrete arguments about which should provide a lower bound in general. We do observe in these cases that the pPF(60, 10)/cc-pVDZ ground-state and polariton energies are visibly lower than the PF-FCI-10/cc-pVDZ energies (see Fig. 5). While the pPF(468, 10)/cc-pVTZ and pPF(2880, 10)/cc-pVQZ also provide ground state and polariton energies below their PF-FCI-10 counterparts, the difference is not visibly discernible (see Figs. 6 and 7). We also note that progression of the Rabi splitting with increasing coupling strength is very comparable between the pPF and PF-FCI results for all basis sets. The pPF(60, 10)/cc-pVDZ result underestimates the Rabi splitting by about 17 meV ($\sim 6 \cdot 10^{-4}$ hartrees) relative to PF-FCI-10/cc-pVDZ, whereas the pPF(2880, 10)/cc-pVQZ result underestimates the splitting by less than 5 meV ($\sim 2 \cdot 10^{-4}$ hartrees) relative to PF-FCI-10/cc-pVQZ. We expect that both methods should agree quite closely in the Rabi splitting because this feature of the polariton states is dominated by the bilinear coupling, and the projected bilinear coupling remains in the same form as its exact counterpart. However, the systematic convergence of the Rabi splitting with increasing basis set size is suggestive of the fact that the dipole self-energy can play a quantitative role in determining the energies of the polariton states, and the error

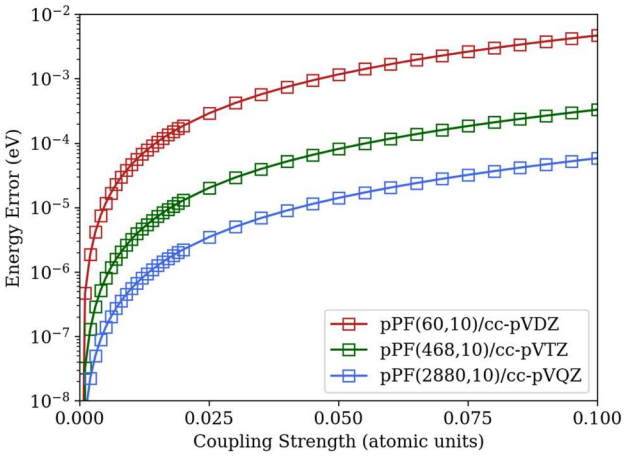

FIG. 3. Absolute error of the ground state energy computed by pPF(N_{el}, 10) relative to PF-FCI-10 computed within the cc-pVDZ, cc-pVTZ, and cc-pVQZ basis sets as a function of coupling strength. For each pPF(N_{el}, 10) result, we choose N_{el} based on the smallest number of electronic states for which the energy error was converged with λ_z = 0.02 a.u., as shown in Fig. 2.

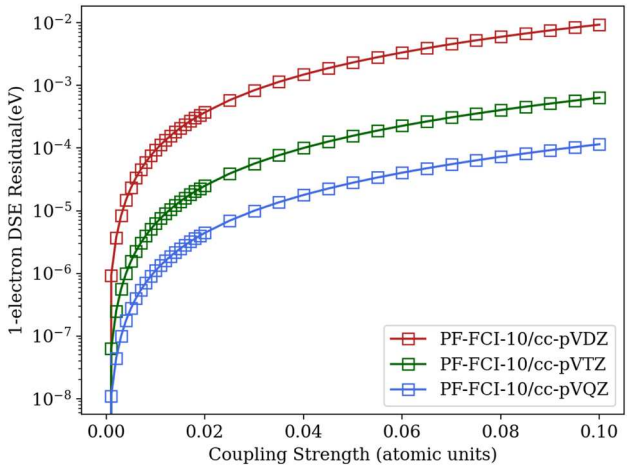

FIG. 4. Ground state residual of the one electron contribution to the dipole self-energy in Eq. (30) as a function of coupling strength for different basis set sizes. The residual rigorously vanishes in the complete basis limit, and we see this trend numerically as we progress from cc-pVDZ through cc-pVQZ.

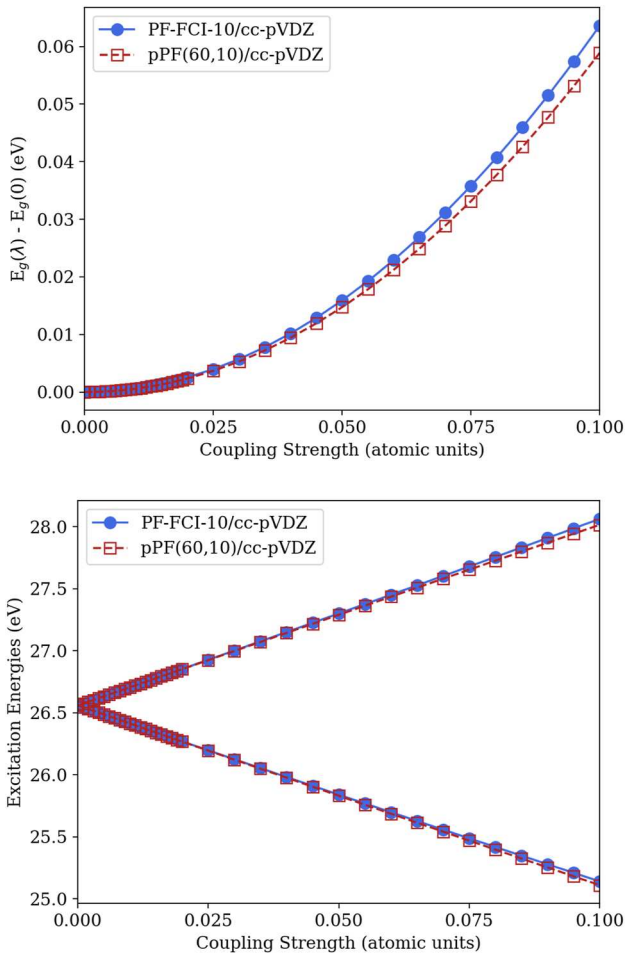

FIG. 5. Relative energy of the ground-state and excitation energies of polariton states of HHe^+ as a function of coupling strength computed at the PF-FCI-10/cc-pVDZ and pPF(60, 10)/cc-pVDZ levels.

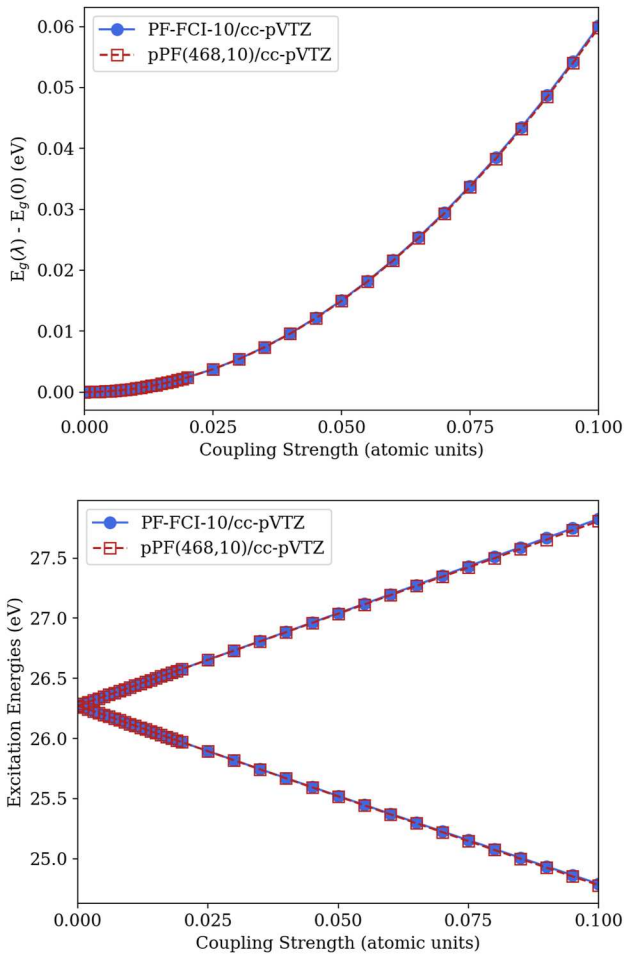

FIG. 6. Relative energy of the ground-state and excitation energies of polariton states of HHe^+ as a function of coupling strength computed at the PF-FCI-10/cc-pVTZ and pPF(468, 10)/cc-pVTZ levels.

in the projected dipole self-energy does not exactly cancel when taking the difference between the polariton energies. We should also note that the errors in the Rabi splitting could be sensitive to the state truncation for the pPF methods that were chosen based on the convergence of the ground state, not the polariton states.

Now that we have shown how the disparity between the pQED and scQED resolves in the complete basis set limit, we can ask a pragmatic question of which requires less computational effort to converge. For this comparison, we use the same direct CI algorithm for the scQED energies as we do for the N_{el} energies and dipole moments required for the pQED results. Although we are typically only interested in a few low-energy eigenstates of Eqs. (1) or (2), as shown in Fig. 2, one often needs to project the pPF Hamiltonian onto many more states than the number of eigenstates that are of interest when the coupling is strong. Because the scQED approach solves Eqs. (1) or (2) directly in a coupled basis, we need only solve for the number of roots of interest. Then, the germane question is how does the effort of solving for the N_{el} adiabatic states required for the lowest N_{ep} coupled states from pQED compare to directly solving for the lowest coupled N_{ep} states from scQED.

In Table III, we present the timings to solve for N_{ep} = 10 coupled states of HeH^+ under the same conditions as shown in Fig. 2 using PF-FCI-10/cc-pVXZ compared to the time required to solve for N_{el} = 40, 312, and 1296 states at the FCI/cc-pVDZ, FCI/cc-pVTZ, and FCI/cc-pVQZ levels, respectively. We choose these N_{el} as 40% of the total roots of the FCI matrix at each basis set, which is approaching the upper limit of what can be performed with our direct CI approach. We note that for the study shown in Fig. 2, we performed full diagonalization of each FCI matrix, not direct CI; this is because the iterative eigensolver used in the direct CI approach generally becomes unsuitable for finding 50% or more of the total eigenvalues of a given matrix. We see that in the cc-pVDZ basis set, it is faster to compute the lowest 40 roots of the FCI matrix than to compute the lowest 10 coupled states. However, the time required for finding the FCI roots increases by roughly 2 orders of magnitude as we progress from cc-pVDZ to cc-pVTZ and again to cc-pVQZ, whereas the time

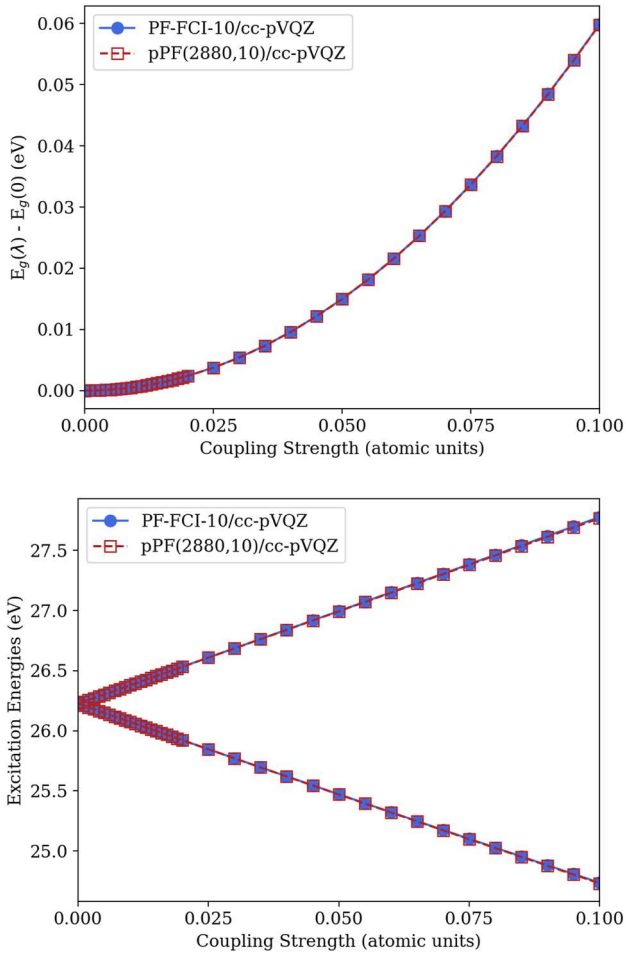

FIG. 7. Relative energy of the ground-state and excitation energies of polariton states of HHe^+ as a function of coupling strength computed at the PF-FCI-10/cc-pVQZ and pPF(2880, 10)/cc-pVQZ levels.

to solve for the lowest 10 coupled PF-FCI roots increases by only 1 order of magnitude for the same progression. Therefore, we see it is ~10× faster to find the lowest 10 roots with PF-FCI-10/cc-pVTZ compared to finding 312 FCI/cc-pVTZ roots, and it is ~100× faster to find the lowest 10 roots with PF-FCI-10/cc-pVQZ than to find the lowest 1296 FCI/cc-pVQZ roots. This scaling is suggestive that it will generally be more computationally facile to directly solve for a small number coupled states in a scQED approach than to solve for a large number of uncoupled states to perform subsequent pQED calculations for the same system size. For example, in recent theoretical studies of ground state modification to the halogenation of nitrobenzene through electronic strong coupling with $|\boldsymbol{\lambda}| \approx 0.1$ a.u., Huo and co-workers found that roughly 100 electronic states were required to converge relative energies to less than 1 kcal/mol;[23] in this case, scQED approaches will likely be more computationally efficient. However, as shown in Fig. 3, state truncation does not yield a significant error when the coupling is relatively small, and so there may be many practical cases of moderate coupling when pQED can be more computationally facile.

TABLE III. Comparison of the time to converge the Davidson iterations for the coupled electronic-photonic roots of the PF-FCI method and the FCI electronic roots of the pPF method for cc-pVDZ, cc-pVTZ, and cc-pVQZ basis sets. For each pPF case, we converge the N_{el} roots chosen to be 40% of the total number of FCI states in that basis. For each PF-FCI case, we solve for the lowest 10 coupled roots with $N_p = 10$ photonic Fock states.

	PF-FCI		pPF	
Basis set	N_p	$t_{convergence}$ (s)	N_{el}	$t_{convergence}$
cc-pVDZ	10	3.4×10^{-2}	40	2.4×10^{-2}
cc-pVTZ	10	4.2×10^{-1}	312	3.5×10^{0}
cc-pVQZ	10	9.2×10^{0}	1296	4.0×10^{2}

B. Lithium hydride (LiH)

The LiH molecule provides a four-electron system that has a permanent ground-state dipole moment and a dipole-allowed optical transition ($S_0 \rightarrow S_1$ with transition energy of 3.29 eV) as seen in Fig. 8. Although we can no longer afford to perform full diagonalization to obtain all FCI many-electron states for the cc-pVXZ series, we can perform FCI (and QED-FCI) in a split-valence triple zeta basis set (6-311G) and obtain hundreds of many-electron states. We will use this system to illustrate the behavior of the pQED and scQED methods in incomplete orbital and many-electron basis limits under strong coupling with $\boldsymbol{\lambda} = (0, 0, 0.05)$ a.u.

We first compute the ground state potential energy scan of LiH at the pPF(500, 2)/6-311G and pPF(500, 10)/6-311G levels of theory, where the latter is fully converged with respect to the size of the electronic and photonic spaces. While we again see that the pPF(500, 10)/6-311G energies are a lower bound to the PF-FCI-10/6-311G energies, we see that the pPF(500, 2)/6-311G energies are an upper bound to the PF-FCI-10/6-311G energies (see Fig. 9). This suggests that the photonic Fock space is incomplete in the latter case. In prior work on scQED approaches, we showed that scQED approaches based on Eq. (2) lead to faster convergence of the photonic Fock space. In Fig. 10, we consider the same potential energy scan and compare the pCS(500, 2)/6-311G and pPF(500, 10)/6-311G levels to PF-FCI-10/6-311G. In this case, we see that the pCS(500, 2)/6-311G energies are indistinguishable from the pPF(500, 10)/6-311G energies, suggesting that the same convergence of the photonic Fock

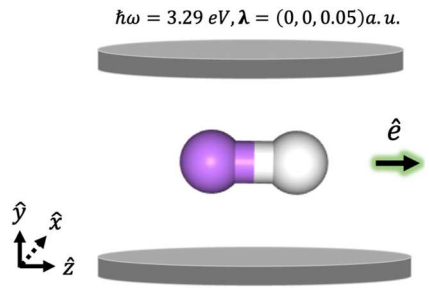

FIG. 8. Schematic of the LiH coupled to a cavity mode polarized along the internuclear axis (z) and tuned to the first optically allowed transition from $S_0 \rightarrow S_1$ at ~3.29 eV.

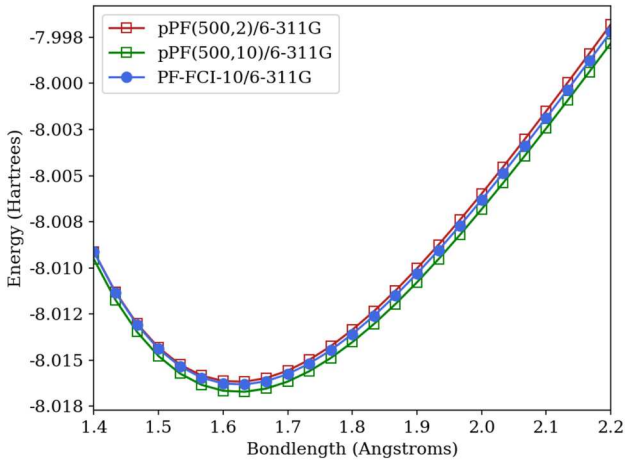

FIG. 9. Ground-state potential energy scan of LiH coupled to a cavity mode with $\lambda = (0, 0, 0.05)$ a.u. and ($\hbar\omega = 3.29$ eV at the pPF(500, 2)/6-311G, pPF(500, 10)/6-311G, and PF-FCI-10/6-311G levels.

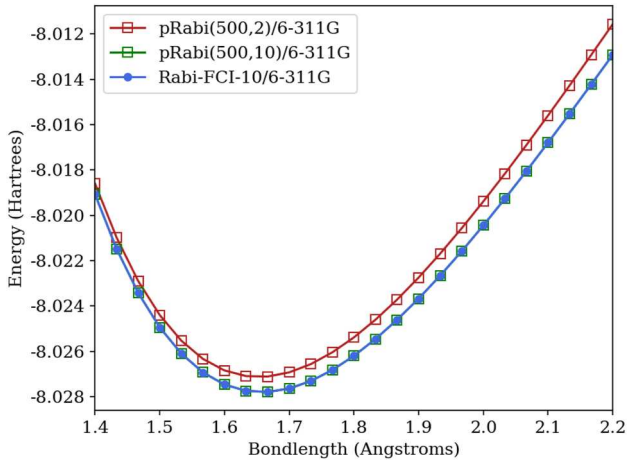

FIG. 11. Ground-state potential energy scan of LiH coupled to a cavity mode with $\lambda = (0, 0, 0.05)$ a.u. and $\hbar\omega = 3.29$ eV at the pRabi(500, 2)/6-311G, pRabi(500, 10)/6-311G, and Rabi-FCI-10/6-311G levels.

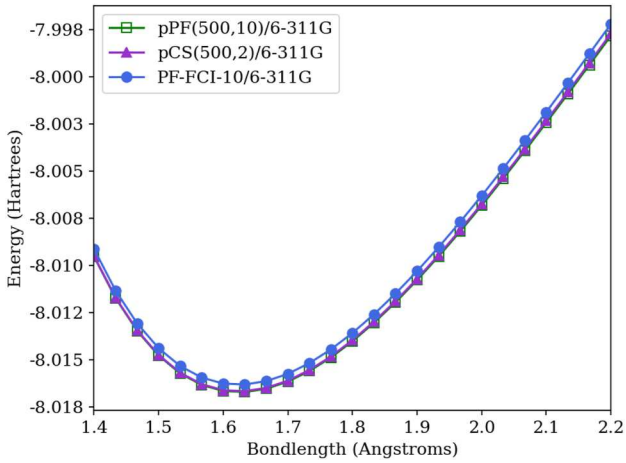

FIG. 10. Ground-state potential energy scan of LiH coupled to a cavity mode with $\lambda = (0, 0, 0.05)$ a.u. and ($\hbar\omega = 3.29$ eV at the pPF(500, 10)/6-311G, pCS(500, 2)/6-311G, and PF-FCI-10/6-311G levels.

space can be realized from the coherent state transformation in pQED approaches as has been observed in scQED approaches.

Finally, we perform the same scan with pQED and scQED approaches that neglect the dipole self-energy operator altogether, which we term pRabi and Rabi-FCI approaches, respectively, to denote the analogy to the Rabi Hamiltonian. In these approaches, the only coupling between the electronic and photonic degrees of freedom arises through the bilinear coupling term. We compute the coupled LiH scan at the pRabi(500, 2)/6-311G, pRabi(500, 10)/6-311G, and Rabi-FCI-10/6-311G levels. Here, we see that the pRabi(500, 2) results are an upper bound to both the pRabi(500, 10) and Rabi-FCI-10 results, which again suggests an incomplete photonic Fock space (see Fig. 11). However, unlike the pPF and PF-FCI results that we have examined so far, the pRabi and Rabi-FCI results are indistinguishable in the limit of a complete photonic Fock space (see Fig. 11). This is consistent with the proposition that the projected bilinear coupling operator agrees with the exact counterpart in a given orbital basis as long as it is projected onto a complete many-electron subspace.

C. Hydroxide ion (OH^-)

The OH^- anion is a charged model system represented within the 6-31G basis set with a bond length of 0.9 Å coupled to a photon with frequency $\hbar\omega_{cav} = 5.96$ eV (0.219 hartrees) polarized along the z axis with $\lambda_z = 0.05$ a.u. We note that this field does not couple directly to a transition in the molecule; while there is a dipole allowed transition at 5.96 eV, in this coordinate system, it does not have a transition dipole moment along the polarization axis of the field. Therefore, the coupling occurs through the permanent dipole moment of the molecule. The number of electronic states used for pCS and pPF calculations is $N_{el} = 50$, and we consider this molecule both with its center of mass located at the cavity origin and displaced by 20 Å from the cavity origin along the z axis, which aligns with the permanent dipole moment and the polarization axis of the field (see Fig. 12). Charged molecules have origin-dependent dipoles[44,64] and this property can lead to numerical difficulties wherein PF-FCI can show origin-dependent energies when the photonic Fock space is incomplete. Our motivation is to examine the behavior of the pPF and PF-FCI methods with systematically increasing photonic Fock spaces and also to investigate if the pCS method is fully origin invariant just like the CS-FCI method. In Fig. 13, we show the origin-dependent energy error for different levels of photonic Fock space truncation using PF-FCI-N_p, pPF(50, N_p), CS-FCI-N_p, and pCS(50, N_p) methods all in the 6-31G basis set. In particular, we define the origin-dependent error as the ground state energy of the displaced system minus the ground state energy of the system at the origin for the same level of truncation. We observe that both PF-FCI and pPF approaches show a remarkably similar

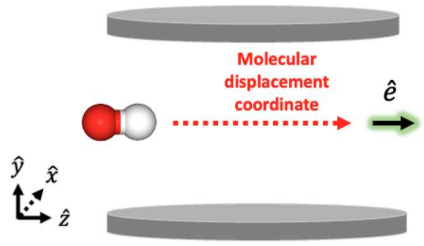

FIG. 12. Schematic of the OH^- displaced from the cavity origin. The cavity mode has the energy of $\hbar\omega = 5.96$ eV with $\lambda_z = 0.05$ a.u., polarized along the internuclear axis of the molecule.

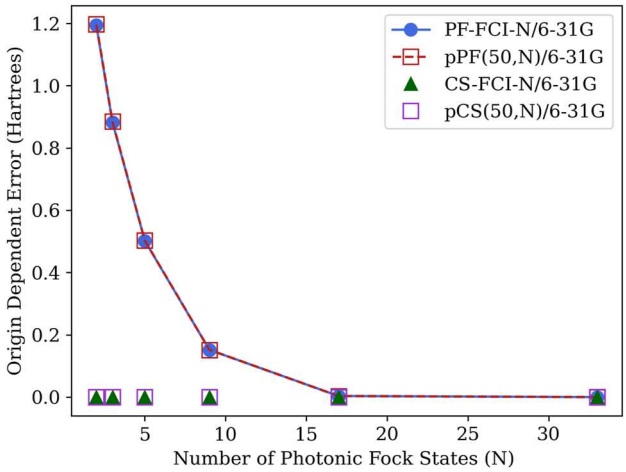

FIG. 13. Origin-dependent energy error of different approaches to computing the OH^- ground state coupled to a cavity mode with $\lambda = (0, 0, 0.05)$ a.u. and $\hbar\omega = 5.96$ eV, where the ions center of mass is displaced by 20 Å from the cavity origin.

origin dependence that converges at the same rate as the photonic Fock space is increased (see Fig. 13). Furthermore, we observe that the pCS and CS-FCI methods are robustly origin invariant (see Fig. 13).

V. CONCLUDING REMARKS

In this work, we have provided a theoretical and numerical comparison of two complementary approaches with ai-QED: (1) parameterized CQED (pQED), a two-step approach where the matter degrees of freedom are computed using existing electronic structure theories, enabling one to build rigorous ai-QED Hamiltonians in a basis of many-electron eigenstates, and (2) self-consistent CQED (scQED), a one-step approach where electronic structure methods are generalized to include coupling between electrons and photon degrees of freedom. Using simple theoretical arguments, we have identified a disparity between the projection of the two-body dipole self-energy operator that appears in the pQED approach and its exact operator counterpart in the scQED approach. We provided a simple theoretical argument that this disparity resolves only in the limit of both complete orbital and many-electron basis for the projection. We provided numerical results highlighting this disparity and its resolution on simple molecular systems, where it is possible to approach these two complete basis limits simultaneously. We also examined and compared the practical issue of computational cost to converge each approach toward the complete orbital and many-electron basis, suggesting that for light–matter coupling strengths that require a large number of electronic states to converge pQED approaches, directly solving for coupled states in scQED approaches will likely be more computationally efficacious. We also examined several situations that highlight that pQED and scQED can show remarkably similar convergence behavior with respect to the photonic Fock space. These findings should provide extremely useful context for the further development and selection of both approaches to strong light–matter coupling.

ACKNOWLEDGMENTS

J.J.F. and R.M. acknowledge the NSF CAREER Award No. CHE-2043215. J.J.F., R.M., and N.V. acknowledge the support from the Center for MAny-Body Methods, Spectroscopies, and Dynamics for Molecular POLaritonic Systems (MAPOL) under subcontract from Grant No. FWP 79715, which is funded as part of the Computational Chemical Sciences (CCS) program by the U.S. Department of Energy, Office of Science, Office of Basic Energy Sciences, Division of Chemical Sciences, Geosciences and Biosciences at Pacific Northwest National Laboratory (PNNL). PNNL is a multi-program national laboratory operated by the Battelle Memorial Institute for the United States Department of Energy under DOE Contract No. DE-AC05-76RL1830. R.M. acknowledges support from the Molecular Sciences Software Institute under U.S. National Science Foundation Grant No. ACI-1547580.

AUTHOR DECLARATIONS

Conflict of Interest

The authors have no conflicts to disclose.

Author Contributions

Ruby Manderna: Formal analysis (equal); Investigation (lead); Methodology (equal); Software (equal); Writing – original draft (equal); Writing – review & editing (equal). **Nam Vu**: Methodology (supporting); Software (equal); Validation (equal); Writing – review & editing (supporting). **Jonathan J. Foley IV**: Conceptualization (lead); Funding acquisition (lead); Methodology (supporting); Resources (lead); Software (supporting); Supervision (lead); Writing – original draft (equal); Writing – review & editing (equal).

DATA AVAILABILITY

The implementation of the QED-CASCI method used for the results presented within can be accessed in the following GitHub repository: https://github.com/mapol-chem/qed-ci/tree/jctc_submission.

The data that support the findings of this study are available from the corresponding author upon reasonable request and are

openly available in GitHub at https://github.com/mapol-chem/qed-ci/tree/jcp_submission.

For HeH^+ data: https://github.com/FoleyLab/data_repository/tree/jcp_submission/Mapol/HHep.

For LiH data: https://github.com/FoleyLab/data_repository/tree/jcp_submission/Mapol/LiH.

For OH^- data: https://github.com/FoleyLab/data_repository/tree/jcp_submission/Mapol/OHminus.

REFERENCES

[1] A. Frisk Kockum, A. Miranowicz, S. De Liberato, S. Savasta, and F. Nori, "Ultrastrong coupling between light and matter," Nat. Rev. Phys. **1**, 19–40 (2019).

[2] J. Flick, N. Rivera, and P. Narang, "Strong light-matter coupling in quantum chemistry and quantum photonics," Nanophotonics **7**, 1479–1501 (2018).

[3] P. Törmä and W. L. Barnes, "Strong coupling between surface plasmon polaritons and emitters: A review," Rep. Prog. Phys. **78**, 013901 (2014).

[4] D. G. Lidzey, D. D. C. Bradley, M. S. Skolnick, T. Virgili, S. Walker, and D. M. Whittaker, "Strong exciton–photon coupling in an organic semiconductor microcavity," Nature **395**, 53–55 (1998).

[5] J. Bellessa, C. Bonnand, J. C. Plenet, and J. Mugnier, "Strong coupling between surface plasmons and excitons in an organic semiconductor," Phys. Rev. Lett. **93**, 036404 (2004).

[6] J. A. Hutchison, T. Schwartz, C. Genet, E. Devaux, and T. W. Ebbesen, "Modifying chemical landscapes by coupling to vacuum fields," Angew. Chem., Int. Ed. **51**, 1592–1596 (2012).

[7] D. M. Coles, Y. Yang, Y. Wang, R. T. Grant, R. A. Taylor, S. K. Saikin, A. Aspuru-Guzik, D. G. Lidzey, J. K.-H. Tang, and J. M. Smith, "Strong coupling between chlorosomes of photosynthetic bacteria and a confined optical cavity mode," Nat. Commun. **5**, 5561 (2014).

[8] E. Orgiu, J. George, J. A. Hutchison, E. Devaux, J. F. Dayen, B. Doudin, F. Stellacci, C. Genet, J. Schachenmayer, C. Genes, G. Pupillo, P. Samorì, and T. W. Ebbesen, "Conductivity in organic semiconductors hybridized with the vacuum field," Nat. Mater. **14**, 1123–1129 (2015).

[9] R. Chikkaraddy, B. de Nijs, F. Benz, S. J. Barrow, O. A. Scherman, E. Rosta, A. Demetriadou, P. Fox, O. Hess, and J. J. Baumberg, "Single-molecule strong coupling at room temperature in plasmonic nanocavities," Nature **535**, 127–130 (2016).

[10] T. W. Ebbesen, "Hybrid light–matter states in a molecular and material science perspective," Acc. Chem. Res. **49**, 2403–2412 (2016).

[11] M. Sukharev and A. Nitzan, "Optics of exciton-plasmon nanomaterials," J. Phys.: Condens. Matter **29**, 443003 (2017).

[12] X. Zhong, T. Chervy, L. Zhang, A. Thomas, J. George, C. Genet, J. A. Hutchison, and T. W. Ebbesen, "Energy transfer between spatially separated entangled molecules," Angew. Chem., Int. Ed. **56**, 9034–9038 (2017).

[13] K. Chevrier, J. M. Benoit, C. Symonds, S. K. Saikin, J. Yuen-Zhou, and J. Bellessa, "Anisotropy and controllable band structure in suprawavelength polaritonic metasurfaces," Phys. Rev. Lett. **122**, 173902 (2019).

[14] S. Kéna-Cohen and S. R. Forrest, "Room-temperature polariton lasing in an organic single-crystal microcavity," Nat. Photonics **4**, 371–375 (2010).

[15] J. Lather, P. Bhatt, A. Thomas, T. W. Ebbesen, and J. George, "Cavity catalysis by cooperative vibrational strong coupling of reactant and solvent molecules," Angew. Chem., Int. Ed. **58**, 10635–10638 (2019).

[16] C. Climent, J. Galego, F. J. Garcia-Vidal, and J. Feist, "Plasmonic nanocavities enable self-induced electrostatic catalysis," Angew. Chem., Int. Ed. **58**, 8698–8702 (2019).

[17] R. K. Yadav, M. Otten, W. Wang, C. L. Cortes, D. J. Gosztola, G. P. Wiederrecht, S. K. Gray, T. W. Odom, and J. K. Basu, "Strongly coupled exciton–surface lattice resonances engineer long-range energy propagation," Nano Lett. **20**, 5043–5049 (2020).

[18] B. Munkhbat, M. Wersäll, D. G. Baranov, T. J. Antosiewicz, and T. Shegai, "Suppression of photo-oxidation of organic chromophores by strong coupling to plasmonic nanoantennas," Sci. Adv. **4**, eaas9552 (2018).

[19] A. E. DePrince III, "Cavity-modulated ionization potentials and electron affinities from quantum electrodynamics coupled-cluster theory," J. Chem. Phys. **154**, 094112 (2021).

[20] A. Mandal, M. A. D. Taylor, B. M. Weight, E. R. Koessler, X. Li, and P. Huo, "Theoretical advances in polariton chemistry and molecular cavity quantum electrodynamics," Chem. Rev. **123**(16), 9786–9879 (2023).

[21] F. Pavošević, S. Hammes-Schiffer, A. Rubio, and J. Flick, "Cavity-modulated proton transfer reactions," J. Am. Chem. Soc. **144**, 4995 (2022).

[22] R. R. Riso, T. S. Haugland, E. Ronca, and H. Koch "Molecular orbital theory in cavity QED environments," Nat. Commun. **13**, 1368 (2022).

[23] B. M. Weight, D. J. Weix, Z. J. Tonzetich, T. D. Krauss, and P. Huo, "Cavity quantum electrodynamics enables *para*- and *ortho*-selective electrophilic bromination of nitrobenzene," J. Am. Chem. Soc. **146**(23), 16184–16193 (2024).

[24] D. Hu and P. Huo, "Ab initio molecular cavity quantum electrodynamics simulations using machine learning models," J. Chem. Theory Comput. **19**, 2353–2368 (2023).

[25] B. M. Weight, T. D. Krauss, and P. Huo, "Investigating molecular exciton polaritons using *ab initio* cavity quantum electrodynamics," J. Phys. Chem. Lett. **14**, 5901–5913 (2023).

[26] J. D. Weidman, M. S. Dadgar, Z. J. Stewart, B. G. Peyton, I. S. Ulusoy, and A. K. Wilson, "Cavity-modified molecular dipole switching dynamics," J. Chem. Phys. **160**, 094111 (2024).

[27] B. G. Peyton, J. D. Weidman, and A. K. Wilson, "Light-induced electron dynamics of molecules in cavities: Comparison of model Hamiltonians," J. Opt. Soc. Am. B **41**, C74–C81 (2024).

[28] M. Ruggenthaler, F. Mackenroth, and D. Bauer, "Time-dependent Kohn-Sham approach to quantum electrodynamics," Phys. Rev. A **84**, 042107 (2011).

[29] I. V. Tokatly, "Time-dependent density functional theory for many-electron systems interacting with cavity photons," Phys. Rev. Lett. **110**, 233001 (2013).

[30] M. Ruggenthaler, J. Flick, C. Pellegrini, H. Appel, I. V. Tokatly, and A. Rubio, "Quantum-electrodynamical density-functional theory: Bridging quantum optics and electronic-structure theory," Phys. Rev. A **90**, 012508 (2014).

[31] C. Pellegrini, J. Flick, I. V. Tokatly, H. Appel, and A. Rubio, "Optimized effective potential for quantum electrodynamical time-dependent density functional theory," Phys. Rev. Lett. **115**, 093001 (2015).

[32] J. Flick, C. Schäfer, M. Ruggenthaler, H. Appel, and A. Rubio, "Ab initio optimized effective potentials for real molecules in optical cavities: Photon contributions to the molecular ground state," ACS Photonics **5**, 992–1005 (2018).

[33] R. Jestädt, M. Ruggenthaler, M. J. T. Oliveira, A. Rubio, and H. Appel, "Light-matter interactions within the Ehrenfest–Maxwell–Pauli–Kohn–Sham framework: Fundamentals, implementation, and nano-optical applications," Adv. Phys. **68**, 225–333 (2019).

[34] J. Flick and P. Narang, "*Ab initio* polaritonic potential-energy surfaces for excited-state nanophotonics and polaritonic chemistry," J. Chem. Phys. **153**, 094116 (2020).

[35] J. McTague and J. J. Foley IV, "Non-Hermitian cavity quantum electrodynamics–configuration interaction singles approach for polaritonic structure with *ab initio* molecular Hamiltonians," J. Chem. Phys. **156**, 154103 (2022).

[36] T. S. Haugland, E. Ronca, E. F. Kjønstad, A. Rubio, and H. Koch, "Coupled cluster theory for molecular polaritons: Changing ground and excited states," Phys. Rev. X **10**, 041043 (2020).

[37] U. Mordovina, C. Bungey, H. Appel, P. J. Knowles, A. Rubio, and F. R. Manby, "Polaritonic coupled-cluster theory," Phys. Rev. Res. **2**, 023262 (2020).

[38] J. Yang, Q. Ou, Z. Pei, H. Wang, B. Weng, Z. Shuai, K. Mullen, and Y. Shao, "Quantum-electrodynamical time-dependent density functional theory within Gaussian atomic basis," J. Chem. Phys. **155**, 064107 (2021).

[39] J. Yang, Z. Pei, E. C. Leon, C. Wickizer, B. Weng, Y. Mao, Q. Ou, and Y. Shao, "Cavity quantum-electrodynamical time-dependent density functional theory within Gaussian atomic basis. II. Analytic energy gradient," J. Chem. Phys. **156**, 124104 (2022).

[40] M. L. Vidal, F. R. Manby, and P. J. Knowles, "Polaritonic effects in the vibronic spectrum of molecules in an optical cavity," J. Chem. Phys. **156**, 204119 (2022).

[41] N. Vu, G. M. McLeod, K. Hanson, and A. E. I. DePrince, "Enhanced diastereocontrol via strong light–matter interactions in an optical cavity," J. Phys. Chem. A **126**, 9303–9312 (2022).

[42]M. D. Liebenthal, N. Vu, and A. E. DePrince III, "Assessing the effects of orbital relaxation and the coherent-state transformation in quantum electrodynamics density functional and coupled-cluster theories," J. Phys. Chem. A **127**, 5264–5275 (2023).
[43]M. Bauer and A. Dreuw, "Perturbation theoretical approaches to strong light–matter coupling in ground and excited electronic states for the description of molecular polaritons," J. Chem. Phys. **158**, 124128 (2023).
[44]N. Vu, D. Mejia-Rodriguez, N. P. Bauman, A. Panyala, E. Mutlu, N. Govind, and J. J. Foley IV, "Cavity quantum electrodynamics complete active space configuration interaction theory," J. Chem. Theory Comput. **20**, 1214–1227 (2024).
[45]B. M. Weight, S. Tretiak, and Y. Zhang, "Diffusion quantum Monte Carlo approach to the polaritonic ground state," Phys. Rev. A **109**, 032804 (2024).
[46]Z.-H. Cui, A. Mandal, and D. R. Reichman, "Variational Lang–Firsov approach plus Møller–Plesset perturbation theory with applications to ab initio polariton chemistry," J. Chem. Theory Comput. **20**, 1143 (2024).
[47]Y. E. Moutaoukal, R. R. Riso, M. Castagnola, and H. Koch, "Toward polaritonic molecular orbitals for large molecular systems," J. Chem. Theory Comput. **20**(20), 8911–8920 (2024).
[48]M. Matoušek, N. Vu, N. Govind, J. J. Foley IV, and L. Veis, "Polaritonic chemistry using the density matrix renormalization group method," J. Chem. Theory Comput. (published online 2024).
[49]M. D. Liebenthal and A. E. DePrince III, "The orientation dependence of cavity-modified chemistry," J. Chem. Phys. **161**(6), 064109 (2024).
[50]M. T. Lexander, S. Angelico, E. F. Kjønstad, and H. Koch, "Analytical evaluation of ground state gradients in quantum electrodynamics coupled cluster theory," J. Chem. Theory Comput. **20**(20), 8876–8885 (2024).
[51]L. Monzel and S. Stopkowicz, "Diagrams and symmetry in polaritonic coupled cluster theory," arXiv:2407.00757 [physics.chem-ph] (2024).
[52]H. Spohn, *Dynamics of Charged Particles and Their Radiation Field* (Cambridge University Press, Cambridge, 2004).
[53]M. Ruggenthaler, N. Tancogne-Dejean, J. Flick, H. Appel, and A. Rubio, "From a quantum-electrodynamical light–matter description to novel spectroscopies," Nat. Rev. Chem **2**, 0118 (2018).
[54]A. Szabo and N. S. Ostlund, "Modern quantum chemistry," in *Introduction to Advanced Electronic Structure Theory*, 1st ed. (Dover Publications, Inc., Mineola, 1996).
[55]R. H. Myhre, T. J. A. Wolf, L. Cheng, S. Nandi, S. Coriani, M. Gühr, and H. Koch, "A theoretical and experimental benchmark study of core-excited states in nitrogen," J. Chem. Phys. **148**, 064106 (2018).
[56]J. J. Foley IV, J. McTague, and A. E. DePrince III, "*Ab initio* methods for polariton chemistry," Chem. Phys. Rev. **4**, 041301 (2023).
[57]M. A. D. Taylor, A. Mandal, W. Zhou, and P. Huo, "Resolution of gauge ambiguities in molecular cavity quantum electrodynamics," Phys. Rev. Lett. **125**, 123602 (2020).
[58]T. Helgaker, P. Jorgensen, and J. Olsen, *Molecular Electronic-Structure Theory* (John Wiley & Sons, 2014).
[59]T. H. Dunning, Jr. and H. Thom, "Gaussian basis sets for use in correlated molecular calculations. I. The atoms boron through neon and hydrogen," J. Chem. Phys. **90**, 1007–1023 (1989).
[60]R. Krishnan, J. S. Binkley, R. Seeger, and J. A. Pople, "Self-consistent molecular orbital methods. XX. A basis set for correlated wave functions," J. Chem. Phys. **72**, 650–654 (1980).
[61]N. Vu, J. J. Foley IV, and R. Manderna, QED-CI: A program for performing cavity quantum electrodynamics configuration interaction calculations, 2023, https://github.com/mapol-chem/qed-ci/tree/main, accessed on July 2024.
[62]D. G. A. Smith, L. A. Burns, D. A. Sirianni, D. R. Nascimento, A. Kumar, A. M. James, J. B. Schriber, T. Zhang, B. Zhang, A. S. Abbott, E. J. Berquist, M. H. Lechner, L. A. Cunha, A. G. Heide, J. M. Waldrop, T. Y. Takeshita, A. Alenaizan, D. Neuhauser, R. A. King, A. C. Simmonett, J. M. Turney, H. F. Schaefer, F. A. Evangelista, A. E. DePrince III, T. D. Crawford, K. Patkowski, and C. D. Sherrill, "Psi4NumPy: An interactive quantum chemistry programming environment for reference implementations and rapid development," J. Chem. Theory Comput. **14**, 3504–3511 (2018).
[63]D. G. A. Smith, L. A. Burns, A. C. Simmonett, R. M. Parrish, M. C. Schieber, R. Galvelis, P. Kraus, H. Kruse, R. Di Remigio, A. Alenaizan, A. M. James, S. Lehtola, J. P. Misiewicz, M. Scheurer, R. A. Shaw, J. B. Schriber, Y. Xie, Z. L. Glick, D. A. Sirianni, J. S. O'Brien, J. M. Waldrop, A. Kumar, E. G. Hohenstein, B. P. Pritchard, B. R. Brooks, H. F. Schaefer, A. Y. Sokolov, K. Patkowski, A. E. DePrince, U. Bozkaya, R. A. King, F. A. Evangelista, J. M. Turney, T. D. Crawford, and C. D. Sherrill, "Psi4 1.4: Open-source software for high-throughput quantum chemistry," J. Chem. Phys. **152**, 184108 (2020).
[64]T. S. Haugland, Strong coupling between localized surface plasmons and molecules by coupled cluster theory, 2019; http://hdl.handle.net/11250/2610781.